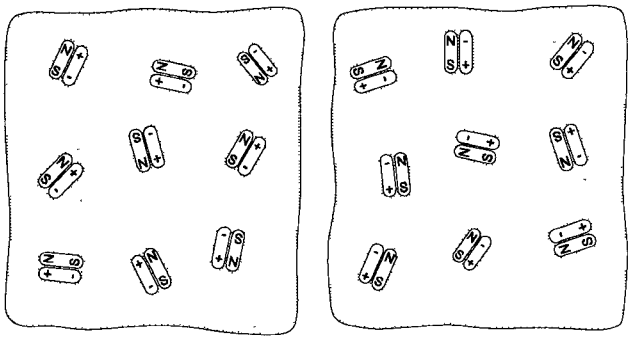

Fig. 2. A phenomenological model for the NRBI Tellegen material. The two samples shown here are isotropic, and have the same magnitude of the nonreciprocity parameter χ but of opposite sign.

This medium evidently is NRBI and violates the result of [1]. There should be no reason why this material could not be built by pivoting the elements on fixed positions within the matrix. The objection can be raised that the interactions between the elements would destroy the isotropy since the symmetry would be spontaneously broken like in permanent magnets. A countermeasure to this danger can be devised by mechanical strings that balance the elements in their original orientations, but which would still allow these to rotate slightly with respect to all three directions in reaction with the incident fields.

Irrespective to the problem of interaction between the elements, one can analyze a single electric-magnetic-dipole pair. This element clearly violates the traceless condition of [1] because its nonreciprocity susceptibility dyadic is uniaxial, being positive for transverse fields and zero for fields along the pair axis. The trace is therefore positive and nonzero.

It is conspicious in this model of Tellegen material that we have to resort to nonelectrical and nonmagnetic forces. This may have some connection to the emphasis in [1] on "physically and chemically stable media" for which the covariance analysis applies. Speculations about unstability of the Tellegen medium also appear in [12], where the asymmetry with respect to time reversal is given as the reason for this.[7]

V. Conclusion

The present article is an attempt to defend the position that NRBI media are not forbidden, at least not because of the covariance principles expounded in [1]. Based on the examples of chromium oxide and phenomenological Tellegen material, the traceless property of the nonreciprocity has been challenged. Since the mathematical derivation leading to the tracelessness in [1] seems to be sound, the arguments of the present paper lead to objections against its starting premise. The inevitable conclusion here is that the covariance property in the form of Post [2] does not hold universally in nature.

Acknowledgment

The author would like to thank the following scientists for useful discussions: J. H. Cloete, B. Jakoby, G. Kristensson, A. Lakhtakia, I. V. Lindell, R. Raab, S. A. Tretyakov, A. Viitanen, W. S. Weiglhofer, and T. B. Yang. Needless to say, the conclusions of the present article are not necessarily shared by these people. I also appreciate the three anonymous reviewers' extensive comments on my original manuscript.

[7]Due to domain nucleation, also simpler media like permanent magnets will eventually decay into the time-symmetric state, thus being unstable. The time constants involved in the process, however, may be millions of years.

References

[1] A. Lakhtakia and W. S. Weiglhofer, "Are linear, nonreciprocal, bi-isotropic media forbidden?" *IEEE Trans. Microwave Theory Tech.*, vol. 42, no. 9, pp. 1715–1716, Sept. 1994.
[2] E. J. Post, *Formal Structure of Electromagnetics.* Amsterdam: North-Holland, 1962, p. 129, (Eq. 6.18).
[3] I. V. Lindell, A. H. Sihvola, S. A. Tretyakov, and A. J. Viitanen, *Electromagnetic Waves in Chiral and Bi-Isotropic Media.* Norwood, Mass: Artech, 1994.
[4] J. A. Kong, *Electromagnetic Wave Theory.* New York: Wiley, 1986, pp. 398–405.
[5] I. E. Dzyaloshinskii, "On the magneto-electrical effects in antiferromagnets," *Soviet Physics JETP*, vol. 10, 1960, pp. 628–629. Dzyaloshinskii's theoretical postulate of the magnetoelectric effect in this material was confirmed by D. N. Astrov, "Magnetoelectric effect in chromium oxide," *Soviet Physics JETP*, vol. 13, no. 4, pp. 729–733, 1961.
[6] V. J. Folen, G. T. Rado, and E. W. Stalder, "Anisotropy of the magnetoelectric effect in Cr_2O_3," *Phys. Review Lett.*, vol. 6, no. 11, pp. 607–608, June 1, 1961.
[7] T. H. O'Dell, *The Electrodynamics of Magneto-Electric Media.* Amsterdam: North-Holland, 1970, p. 282.
[8] R. Raab, private communication.
[9] T. H. O'Dell, "Measurements of the magneto-electric susceptibility of polycrystalline chromium oxide," *Philisophical Magazine*, vol. 13, pp. 921–933, 1966.
[10] A. Sihvola, "When doubting Tellegen material give her the benefit of the doubt," *Chiral discussion forum* `CHIRAL-L` *at* `listserv@DEARN.BITNET` *alias* `listserv@VM.GMD.DE`, on 21 Dec. 1994.
[11] B. D. F. Tellegen. "The gyrator, a new electric network element," *Philips Res. Rep.*, vol. 3, no. 2, 1948, pp. 81–101.
[12] Reference [7], pp. 11, 18.

Fourier-Transform Analysis for Rectangular Groove Guide

Byung-Tak Lee, Jae W. Lee, Hyo J. Eom, and Sang-Yung Shin

***Abstract*—The rectangular groove guide is analyzed using the Fourier transform and the mode-matching technique. The enforcement of the boundary conditions at the groove apertures yields the simultaneous equations for the field coefficient inside the grooves. The simultaneous equations are solved to represent a dispersion relation in analytic series form. The numerical computation is performed to illustrate the behavior of the guided wave in terms of frequency and groove sizes. The presented series solution is exact and rapidly-convergent so that it is efficient for numerical computation. A simple dispersion relation based on the dominant-mode analysis is obtained and is shown to be very accurate for most practical applications.**

Manuscript received July 20, 1994; revised May 25, 1995.

The authors are with the Department of Electrical Engineering, Korea Advanced Institute of Science and Technology, 373-1, Kusong Dong, Yusung Gu, Taejon, Korea.

IEEE Log Number 9413414.

I. Introduction

The groove guide is a useful structure due to its low-loss high-power capacity above 100 GHz. Experimental studies were performed in [1] to determine the dispersion relation of the groove guide. Theoretical studies were also performed using the approximate equivalent network [2] and the numerical approach [3]. Although the dispersion relation of the groove guide has been relatively well understood, it is of interest to obtain an exact analytic solution. In this paper, we obtain such a solution by utilizing the Fourier transform and mode-matching. The solution is in rapidly-convergent series so that it is very efficient for numerical computation. In low-frequency limit, the solution simplifies yielding a dominant-mode approximate dispersion relation which is very accurate for most practical applications. In the next sections, we derive the dispersion relations for the TM and TE modes and discuss the numerical efficiency of our solution. The notations used in the paper closely follow those in [5].

II. Field Representations

Assume a TE or TM mode propagates along the z direction inside the groove guide in Fig. 1. With the time-factor $e^{j\omega t}$ suppressed the propagating E-field $\overline{E}(x, y, z)$ is given as $\overline{E}(x, y)e^{-j\beta z}$. In regions (I), (II), and (III) E_z and H_z are

$$E_z^I(x, y) = \sum_{m=1}^{\infty} p_m \sin a_m(x + a) \cdot \sin \xi_m(y + d) \tag{1}$$

$$H_z^I(x, y) = \sum_{m=0}^{\infty} q_m \cos a_m(x + a) \cdot \cos \xi_m(y + d) \tag{2}$$

$$E_z^{II}(x, y) = \frac{1}{2\pi} \int_{-\infty}^{\infty} \cdot (\tilde{E}_z^+ e^{j\kappa y} + \tilde{E}_z^- e^{-j\kappa y}) e^{-j\zeta x}\, d\zeta \tag{3}$$

$$H_z^{II}(x, y) = \frac{1}{2\pi} \int_{-\infty}^{\infty} \cdot (\tilde{H}_z^+ e^{j\kappa y} + \tilde{H}_z^- e^{-j\kappa y}) e^{-j\zeta x}\, d\zeta \tag{4}$$

$$E_z^{III}(x, y) = \sum_{m=1}^{\infty} r_m \sin a_m(x + a) \cdot \sin \xi_m(y - b - d) \tag{5}$$

$$H_z^{III}(x, y) = \sum_{m=0}^{\infty} s_m \cos a_m(x + a) \cdot \cos \xi_m(y - b - d) \tag{6}$$

where $a_m = m\pi/(2a)$, $\xi_m = \sqrt{k^2 - a_m^2 - \beta^2}$, $\kappa = \sqrt{k^2 - \beta^2 - \zeta^2} \equiv \sqrt{k_c^2 - \zeta^2}$, $k = \omega\sqrt{\mu\epsilon} = 2\pi/\lambda$: wave number. The remaining field components are immediate from

$$E_x^v = \frac{-j}{k_t^2}\left(\frac{\beta \partial E_z^v}{\partial x} + \omega\mu \frac{\partial H_z^v}{\partial y}\right) \tag{7}$$

$$E_y^v = \frac{-j}{k_t^2}\left(\frac{\beta \partial E_z^v}{\partial y} - \omega\mu \frac{\partial H_z^v}{\partial x}\right) \tag{8}$$

$$H_x^v = \frac{-j}{k_t^2}\left(\frac{\beta \partial H_z^v}{\partial x} - \omega\epsilon \frac{\partial E_z^v}{\partial y}\right) \tag{9}$$

$$H_y^v = \frac{-j}{k_t^2}\left(\frac{\beta \partial H_z^v}{\partial y} + \omega\epsilon \frac{\partial E_z^v}{\partial x}\right) \tag{10}$$

where v = I, II, III, and $k_t^2 = k^2 - \beta^2$.

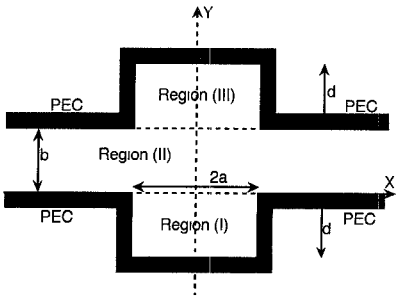

Fig. 1. Geometry of rectangular groove guide.

III. TM-Mode Analysis

We consider the TM-case, $E_z \neq 0$ and $H_z = 0$. The enforcement of the boundary conditions is necessary to determine unknown coefficients p_m and r_m.

The condition $E_z^{II}(x, 0) = E_z^I(x, 0)$ gives

$$\frac{1}{2\pi}\int_{-\infty}^{\infty} (\tilde{E}_z^+ + \tilde{E}_z^-) e^{-j\zeta x}\, d\zeta = \begin{cases} \sum_{m=1}^{\infty} p_m \sin a_m(x + a) \sin(\xi_m d) & \text{for } |x| < a \\ 0 & \text{for } |x| > a. \end{cases} \tag{11}$$

Taking the Fourier transform of (11), we obtain

$$\tilde{E}_z^+ + \tilde{E}_z^- = \sum_{m=1}^{\infty} p_m a_m \sin(\xi_m d) a^2 F_m(\zeta a) \tag{12}$$

where $E_z^{II}(x, 0)$ and $\tilde{E}_z^+ + \tilde{E}_z^-$ are a Fourier transform pair and

$$F_m(g) = \frac{e^{jg}(-1)^m - e^{-jg}}{g^2 - (m\pi/2)^2}. \tag{13}$$

The condition $H_x^{II}(x, 0) = H_x^I(x, 0)$ for $|x| < a$ gives

$$\frac{1}{2\pi}\int_{-\infty}^{\infty} j\kappa(\tilde{E}_z^+ - \tilde{E}_z^-) e^{-j\zeta x}\, d\zeta = \sum_{m=1}^{\infty} p_m \xi_m \sin a_m(x + a) \cos(\xi_m d). \tag{14}$$

Similarly the condition $E_z^{III}(x, b) = E_z^{II}(x, b)$ gives

$$\tilde{E}_z^+ e^{j\kappa b} + \tilde{E}_z^- e^{-j\kappa b} = -\sum_{m=1}^{\infty} r_m a_m \sin(\xi_m d) a^2 F_m(\zeta a). \tag{15}$$

The condition $H_x^{III}(x, b) = H_x^{II}(x, b)$ for $|x| < a$ gives

$$\frac{1}{2\pi}\int_{-\infty}^{\infty} j\kappa(\tilde{E}_z^+ e^{j\kappa b} - \tilde{E}_z^- e^{-j\kappa b}) e^{-j\zeta x}\, d\zeta = \sum_{m=1}^{\infty} r_m \xi_m \sin a_m(x + a) \cos(\xi_m d). \tag{16}$$

Eliminating $\tilde{E}_z^+$ and $\tilde{E}_z^-$ from (12), (14), (15), and (16) we obtain

$$\sum_{m=1}^{\infty} p_m \xi_m \cos(\xi_m d) \sin a_m(x + a) = \frac{1}{2\pi}\int_{-\infty}^{\infty} \kappa[-A \cot(\kappa b) + B \csc(\kappa b)] e^{-j\zeta x}\, d\zeta \tag{17}$$

$$\sum_{m=1}^{\infty} r_m \xi_m \cos(\xi_m d) \sin a_m(x + a) = \frac{1}{2\pi}\int_{-\infty}^{\infty} \kappa[-A \csc(\kappa b) + B \cot(\kappa b)] e^{-j\zeta x}\, d\zeta \tag{18}$$

where

$$A = \sum_{m=1}^{\infty} p_m a_m \sin(\xi_m d) a^2 F_m(\zeta a) \tag{19}$$

$$B = -\sum_{m=1}^{\infty} r_m a_m \sin(\xi_m d) a^2 F_m(\zeta a). \tag{20}$$

Multiplying (17) and (18) by $\sin a_n(x+a)$ and integrating from $-a$ to a, we obtain

$$\sum_{m=1}^{\infty} p_m \left[\frac{4a\xi_m}{(m\pi)^2}\cos(\xi_m d)\delta_{mn} + \sin(\xi_m d) I_{1,mn}\right] + r_m \sin(\xi_m d) I_{2,mn} = 0 \tag{21}$$

$$\sum_{m=1}^{\infty} p_m \sin(\xi_m d) I_{2,mn} + r_m \cdot \left[\frac{4a\xi_m}{(m\pi)^2}\cos(\xi_m d)\delta_{mn} + \sin(\xi_m d) I_{1,mn}\right] = 0 \tag{22}$$

where δ_{mn} is the Kronecker delta and

$$I_{1,mn} = \frac{1}{2\pi}\int_{-\infty}^{\infty} a^2\kappa \cot(\kappa b) \cdot F_m(\zeta a) F_n(-\zeta a)\, d\zeta \tag{23}$$

$$I_{2,mn} = \frac{1}{2\pi}\int_{-\infty}^{\infty} a^2\kappa \csc(\kappa b) \cdot F_m(\zeta a) F_n(-\zeta a)\, d\zeta. \tag{24}$$

Using the residue calculus, we evaluate $I_{1,mn}$ and $I_{2,mn}$

$$I_{1,mn} = \begin{cases} \dfrac{4a\xi_m \cot(\xi_m b)}{(m\pi)^2}\delta_{mn} - j\displaystyle\sum_{v=1}^{\infty} U_{mn}\left(\frac{v\pi}{b}\right) & m+n = \text{even} \\ 0 & m+n = \text{odd} \end{cases} \tag{25}$$

$$I_{2,mn} = \begin{cases} \dfrac{4a\xi_m \csc(\xi_m b)}{(m\pi)^2}\delta_{mn} - j\displaystyle\sum_{v=1}^{\infty} (-1)^v U_{mn}\left(\frac{v\pi}{b}\right) & m+n = \text{even} \\ 0 & m+n = \text{odd} \end{cases} \tag{26}$$

where

$$U_{mn}(g) = \frac{2}{a^2 b}\frac{g^2}{\sqrt{k^2-\beta^2-g^2}} \cdot \frac{1-(-1)^m e^{j2\sqrt{k^2-\beta^2-g^2}a}}{(\xi_m^2-g^2)(\xi_n^2-g^2)}. \tag{27}$$

Substitution of (25) and (26) into (21) and (22) yields

$$\begin{bmatrix} \Psi_1 & \Psi_2 \\ \Psi_2 & \Psi_1 \end{bmatrix}\begin{bmatrix} P \\ R \end{bmatrix} = \begin{bmatrix} 0 \\ 0 \end{bmatrix} \tag{28}$$

where the elements of Ψ_1 and Ψ_2 for $m+n =$ even are

$$\psi_{1,mn} = \frac{4a\xi_m}{(m\pi)^2}\left[\cos(\xi_m d) + \sin(\xi_m d)\cot(\xi_m b)\right] \cdot \delta_{mn} - j\sin(\xi_m d)\sum_{v=1}^{\infty} U_{mn}\left(\frac{v\pi}{b}\right) \tag{29}$$

$$\psi_{2,mn} = \frac{4a\xi_m}{(m\pi)^2}\sin(\xi_m d)\csc(\xi_m b)\delta_{mn} - j\sin(\xi_m d) \cdot \sum_{v=1}^{\infty}(-1)^v U_{mn}\left(\frac{v\pi}{b}\right). \tag{30}$$

TABLE I
CONVERGENCE BEHAVIOR WITH CHANGING GROOVE DEPTH ($a = 1.2$ cm, $b + 2d = 2$ cm, $f = 10$ GHz)

matrix size	2×2 Eq (33)	6×6 Eq (33)	10×10 Eq (33)	simple solution Eq (37)	12×12 Inderjit[3]
$b/2$[cm]	λ/λ_g, λ_g guide wavelength				
0.1	0 6595	0 6595	0 6595	0 6595	0 6598
0 2	0 6539	0 6538	0 6535	0 6539	0 6535
0 3	0 6449	0 6442	0 6436	0 6449	0 6433
0 4	0 6330	0 6316	0 6306	0 6330	0 6300
0 5	0 6194	0 6169	0 6156	0 6194	0 6149
0 6	0 6058	0 6025	0 6011	0 6058	0 6005
0 7	0 5952	0 5921	0 5909	0 5952	0 5906
0 8	0 5930	0 5910	0 5903	0 5930	0 5906
0 9	0 6084	0 6080	0 6078	0 6084	0 6090

The requirement that the determinant be zero gives

$$\begin{vmatrix} \Psi_1 & \Psi_2 \\ \Psi_2 & \Psi_1 \end{vmatrix} = 0. \tag{31}$$

In low-frequency limit, (31) simplifies to a dominant-mode ($m = 1$) approximate solution

$$\psi_{1,11} - \psi_{2,11} = 0. \tag{32}$$

Similarly, it is possible to consider the TE-case by assuming $E_z = 0$ and $H_z \neq 0$. The results are summarized here. The dispersion relation for the TE-mode is

$$\begin{vmatrix} \Psi_3 & \Psi_4 \\ \Psi_4 & \Psi_3 \end{vmatrix} = 0 \tag{33}$$

where for $m+n =$ even

$$\psi_{3,mn} = \frac{\varepsilon_m}{a\xi_m}\left[\cos(\xi_m d) + \sin(\xi_m d)\cot(\xi_m b)\right] \cdot \delta_{mn} - j\sin(\xi_m d)\sum_{v=0}^{\infty}\frac{1}{\varepsilon_v} V_{mn}\left(\frac{v\pi}{b}\right) \tag{34}$$

$$\psi_{4,mn} = \frac{\varepsilon_m}{a\xi_m}\sin(\xi_m d)\csc(\xi_m b)\delta_{mn} - j\sin(\xi_m d) \cdot \sum_{v=0}^{\infty}\frac{(-1)^v}{\varepsilon_v} V_{mn}\left(\frac{v\pi}{b}\right) \tag{35}$$

$$V_{mn}(g) = \frac{2}{a^2 b}\sqrt{k^2-\beta^2-g^2} \cdot \frac{1-(-1)^m e^{j2\sqrt{k^2-\beta^2-g^2}a}}{(\xi_m^2-g^2)(\xi_n^2-g^2)} \tag{36}$$

and $\varepsilon_m = 2(m=0), 1(m = 1, 2, 3, \ldots)$.

A dominant-mode approximate solution is

$$\psi_{3,00} - \psi_{4,00} = 0.$$

We check the convergence behavior of our solution λ/λ_g in Table I which shows that our solution (33) agrees well with [3] and converges very fast. The dominant-mode approximate solution (37) also yields accurate results for practical purposes. Fig. 2 shows the theoretical behavior of the cutoff wavelength λ_c for the TE and TM-modes using (32) and (37). As expected, the cutoff wavelength for the TE-mode is much larger than that for the TM-mode. Our TE-mode solution agrees well with the improved solution in [2]. The numerical computations in Table I and Fig. 2 illustrate that our approximate dispersion relations (32) and (37) are simple yet accurate for all practical waveguide geometries considered in [1]–[3].

IV. CONCLUSION

The problem of the rectangular groove guide is solved using the Fourier transform. The solution is presented in fast-convergent series form which is efficient for numerical computation. The dominant-

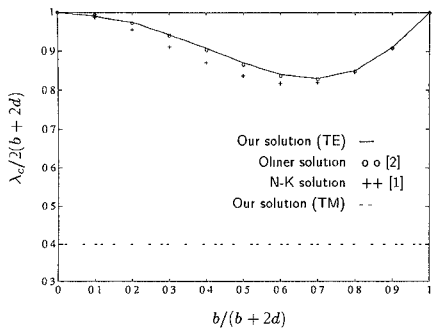

Fig. 2. Theoretical values of $\lambda_c/2(b+2d)$ versus relative width $b/(b+2d)$ of groove, where λ_c is the cutoff wavelength and $a/(b+2d) = 0.2$.

mode approximate solutions are obtained in low-frequency limit and are shown to be accurate for most practical applications.

REFERENCES

[1] T. Nakahara and N. Kurauchi, "Transmission modes in the grooved guide," *J. Inst. Electron. Commun. Eng. Jap.*, vol. 47, no. 7, pp. 43–51, July 1964.

[2] A. A. Oliner and P. Lampariello, "The dominant mode properties of open groove guide: An improved solution," *IEEE Trans. Microwave Theory Tech.*, vol. MTT-33, pp. 755–764, Sept. 1985.

[3] Inderjit and M. Sachidananda, "Rigorous analysis of a groove guide," *IEE Proc.-H*, vol. 139, no. 5, pp. 449–452, Oct. 1992.

[4] M. Zhewang, Y. Eikichi, and X. Shanjia, "Modal analysis of open groove guide with arbitrary groove profile," *IEEE Microwave and Guided Wave Lett.*, vol. 2, no. 9, pp. 364–366, Sept. 1992.

[5] T. J. Park, H. J. Eom, and K. Yoshitomi, "An analysis of transverse electric scattering from a rectangular channel in a conducting plane," *Radio Sci.*, vol. 28, no. 5, pp. 663–673, Sept.–Oct. 1993.

Phasor Diagram Analysis of Millimeter-Wave HEMT Mixers

Youngwoo Kwon and Dimitris Pavlidis

***Abstract*—A phasor diagram method is developed based on an analytic approach for conversion gain evaluation in HEMT mixers. The analytical expressions derived in this work take into account the mixing terms of nonlinear elements and provide a simple method to evaluate the conversion gain. The phasor diagram analysis offers physical insight into the mixing mechanisms and identifies the role of each harmonic of the nonlinear elements of HEMT's on the conversion gain. The method is validated with the experimental data of W-band monolithic InP-based HEMT mixers.**

I. INTRODUCTION

HEMT's are promising nonlinear devices for mixers due to their highly nonlinear transconductance characteristics, as well as their conversion gain capability. Recently, HEMT mixers have been realized up to 94 GHz using InAlAs/InGaAs heterostructures [1], [2]. However, the complicated nature of their equivalent circuits and highly nonlinear characteristics make their analysis and optimization difficult. General mixer design and analysis methods were presented in [3] and [4]. HEMT mixer design is usually based on harmonic balance techniques available nowadays in commercial software packages such as Libra of EEsof. The design procedure involves, in this case, consideration of the HEMT equivalent circuit, and definition of the input and output terminations. Based on these, one can evaluate parameters such as the conversion gain at the intermediate frequencies under various input power levels. Furthermore, it is necessary to understand the role of each nonlinear element and its higher order intermixing terms on the conversion gain in HEMT mixers. In this paper, an analytical expression for the conversion gain is derived using a simplified equivalent circuit model. A phasor diagram analysis is presented, showing the mixing components from each nonlinear element and its higher harmonics. This allows one to obtain physical insight into the mixing mechanisms and provides a simple analytical expression for evaluating and optimizing conversion gain.

Manuscript received September 16, 1994; revised May 25, 1995. This work was supported by URI Contract DAAL 03-92-G-0109.

Y. Kwon was with the Department of Electrical Engineering and Computer Science, University of Michigan, Ann Arbor, MI. He is now with Rockwell Science Center, Thousand Oaks, CA 91360 USA.

D. Pavlidis is with the Department of Electrical Engineering and Computer Science, University of Michigan, Ann Arbor, MI 48109-2122 USA.

IEEE Log Number 9413422.

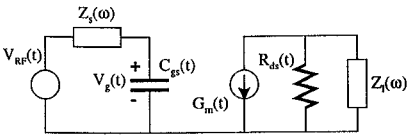

Fig. 1. Simplified equivalent circuit of HEMT mixers used in the phasor diagram analysis.

II. SIMPLIFIED HEMT MIXER THEORY

First, the nonlinearities of the HEMT's are investigated using a combination of a single-tone Harmonic Balance and FFT techniques. The circuit configuration for the calculation was based on the simplified equivalent circuit model of HEMT mixers shown in Fig. 1. Three elements are considered to be nonlinear and participate in the mixing mechanism: C_{gs}, G_m, and R_{ds}. The other elements are taken to be linear and included in the $Z_s(\omega)$ and $Z_l(\omega)$ impedances. The harmonic generation of these three nonlinear elements are investigated as a function of LO power. For this purpose, the device was pumped with a single-tone variable-power LO signal and the time-dependent data of the intrinsic nonlinear parameters were calculated. These time-domain data were then transformed to the frequency-domain data using FFT. Among the three elements, G_m showed the largest harmonic generation. Fig. 2 describes the frequency domain data of G_m as a function of LO power for a 0.1 μm-long, 90 μm-wide gate HEMT using InAlAs/InGaAs heterojunction [5]. The generation of the first harmonic component of G_m (G_{m_1}) is significant at high LO power levels and decreases after a certain power level due to "parasitic MESFET" operation, as shown in [2]. This component is later shown to be most responsible for the mixing mechanism.

Based on the above considerations, an analytical expression is derived for the conversion gain according to the following assumptions and termination conditions:

1) The gate port is short-circuited at the "IF" frequency and only the "Image" and "RF" frequencies are allowed. The higher order harmonics are assumed to be negligibly small, a condition which is satisfied, provided that a proper termination is present